2015 IEEE/RSJ International Conference on Intelligent Robots and Systems (IROS)
Congress Center Hamburg
Sept 28 - Oct 2, 2015. Hamburg, Germany

A Fast Histogram-Based Similarity Measure for Detecting Loop Closures in 3-D LIDAR Data

Timo Röhling, Jennifer Mack, and Dirk Schulz
Fraunhofer FKIE, Fraunhoferstr. 20, 53343 Wachtberg, Germany

***Abstract*— We present a fast method of detecting loop closure opportunities through the use of similarity measures on histograms extracted from 3-D LIDAR data. We avoid computationally expensive features and compute histograms over simple global statistics of the LIDAR scans. The resulting histograms encode sufficient information to detect spatially close scans with high precision and recall and can be computed at rates faster than data acquisition on modest consumer-grade hardware. Our approach is able to match previously established results in LIDAR loop closure detection with less computational overhead.**

I. Introduction

Field robots are increasingly being used in environments of greater complexity, including areas where Global Navigation Satellite Systems (GNSS) or other means of reliable localisation are not available. This includes disaster zones and dense forests or jungles. In such instances, sensor-based localisation may be used to augment an Inertial Measurement Unit (IMU) or other dead reckoning sensors. Scan matching and visual odometry are popular methods of achieving this purpose. However, being locally optimal, these methods cause a drift in position, which is undesirable for larger-area mission planning scenarios where the robots are expected to revisit places. In order to achieve global optimality, many solutions have been proposed. Specifically, loop closure detection algorithms have been developed to bound positioning errors caused by drift in sensors or incremental localisation methods. Loop closure can be defined as a specialisation of the data association problem which contributes to the discrete uncertainty in Simultaneous Localization and Mapping (SLAM) problems.

SLAM algorithms which keep the full pose posterior can find the global optimum in the solution space and do not suffer from the loop closure problem. Algorithms based on particle filters are well-suited for this task and are frequently employed to solve SLAM in 2-D. However, it is virtually impossible to represent the full posterior for 3-D maps with the necessary accuracy, even for small map sizes. Locally optimal estimation methods exploit that the posterior can never be influenced by features outside the sensor range, and decompose the posterior into a sparse graph. The graph nodes represent locations and are annotated with sensor information, the edges encode pose constraints between two nodes. While it is trivial to connect nodes in the order they were visited, the accumulating residual error makes it very difficult to detect if a previously recorded node is being revisited, given a sufficiently large loop.

The general framework of our solution is to use scan matching as a basis for incremental localisation. The seed to the scan matching algorithm could be an identity transformation matrix, an input from an IMU or encoder, or the results of previous iterations of the algorithm. We implement a vanilla 3-D ICP algorithm on the entire point cloud. The discussion of scan matching is beyond the scope of this paper. Next, a "fingerprint" is taken of the 3-D point cloud, using our novel similarity measure. It was observed that the histograms exhibit certain characteristics: They are invariant to position and orientation, barring occlusion problems inherent in LIDAR sensors. They are also fast to compute and are thus suitable for online applications.

The remainder of the paper is organized as follows: In section II, we present the current state of the art in the field of robotics regarding loop closure. In section III, we introduce the technical details of our histogram measure and discuss the theoretical advantages and disadvantages. In section IV, we give the results of our experimental evaluation with real-world data. We finish with a few concluding thoughts and an outlook on our future work in section V.

II. Related Work

Loop closure (at times known as the revisiting problem) algorithms have been frequently studied when globally optimal localisation solutions are required. We define loop closure as a specialisation of data association [1], where a position has to be corresponded with another that has been previously visited. We further argue that in loop closure problems, false positives in detection are often irrecoverable and cause filter divergence almost immediately.

Gated nearest neighbour methods using Euclidean or Mahalanobis distance – usually integrated with EKF-SLAM – are often inadequately robust for loops of significant sizes. Hence, various researches have surfaced on alternative methods. In vision-based localisation, the use of SIFT [2] and SURF [3] has been attempted to detect similarities in the feature space of images. FrameSLAM [4] is a more real-time technique that forms the basis for CenSurE [5].

In GraphSLAM methods, various approaches have been applied to loop closure detection. Gutmann and Konolige [6] use a heuristic-based filter on the probability of a 2-D map patch being similar to the current local map patch while considering the Unmanned Ground Vehicle's (UGV) current position and covariance. Another heuristic approach is Sprickerhof et al. [7].

978-1-4799-9994-1/15/$31.00 ©2015 IEEE

Neira and Tardos [8] propose an improvement to the gated nearest neighbour by considering all associations simultaneously in the complete set of features; Nieto et al. [9] and Wijesoma et al. [10] track multiple hypotheses to increase the robustness against data association errors. Other methods that operate in feature space include Bailey et al. [11] and Stewart et al [12]. Pfaff et al. [13] consider a dense set of features in a multi-level surface map and identify loop closures based on the Mahalanobis distance. Entropy-based loop closure detection on sets of features is proposed by Folkesson and Christensen [14], where the increase in energy due to matching two feature sets (which can be distant from each other metrically) is used to determine if a loop closure event has occurred.

Magnusson et al. [15] introduce the Normal Distribution Transform (NDT) to capture structural information in LIDAR scans. Initially developed as a means for scan registration, histograms of NDT descriptors provide sufficient structural information for a robust loop closure detection with very few false positives. Each LIDAR scan is spatially divided into overlapping cells. For each cell, the Normal Distribution Transform is computed. The number of instances for certain shape classes of NDTs in each of five range intervals constitute the histogram. Histograms are compared using a weighted Euclidean distance metric. As the approach is closely related to our own, we will use the NDT performance as baseline for our evaluation. We will show that the histogram technique is a powerful method independent of the NDT algorithm; in fact, the results of Magnusson et al. can be reproduced with our simpler histogram types and a different distance metric.

III. LIDAR Histograms

A. Definition

For our purposes, LIDAR data is assumed to be recorded as scans, where each scan is represented as an unstructured 3-D point cloud and associated with a location. Usually, one scan corresponds to one full rotation of the measuring head. For low speeds, the robot can be regarded stationary during a single scan, or one can compensate for the motion when projecting the distance measurements into the cartesian space.

Our histogram algorithm utilizes a point projection function $v\colon \mathbb{R}^3 \to \mathbb{R}$ that assigns a real number to a point, effectively projecting the LIDAR scan data to a single dimension. An example for such a function would be the distance between the point and the robot. While it would be possible to create a multi-dimensional histogram from the actual points, the computation of the difference between two histograms becomes quite involved and is actually less robust.

The histogram is a normalized discretization of the function's value range. Assuming a bucket count b and a value range $I = [v_{\min}, v_{\max}]$, we divide I into subintervals of size

$$\Delta I_b = \frac{1}{b}\left(v_{\max} - v_{\min}\right), \tag{1}$$

so each bucket corresponds with one of the disjunct intervals

$$I_b^k = \left[v_{\min} + k \cdot \Delta I_b, v_{\min} + (k+1) \cdot \Delta I_b\right[. \tag{2}$$

Then, the histogram for a scan S can be written as

$$H_b = \left(h_b^0, \ldots, h_b^{b-1}\right) \tag{3}$$

with

$$h_b^k = \frac{1}{|S|}\left|\left\{p \in S\colon v(p) \in I_b^k\right\}\right|. \tag{4}$$

Under ideal circumstances, the number of LIDAR measurements per scan will be constant. In practise, rotating devices have slight variations in their angular velocity, and some surface types (e.g. water) may not return any meaningful measurements at all if hit at certain angles. The normalization ensures that the histograms remain comparable even under these adverse conditions.

For the histogram comparison, we employ the discrete Wasserstein metric between two histograms G_b and H_b

$$\mathcal{W}(G_b, H_b) = \min_{\sigma \in \Sigma_0^b} \sum_i \frac{1}{b}\left|(i - \sigma(i))\left(g_b^i - h_b^{\sigma(i)}\right)\right| \tag{5}$$

with Σ_0^b being the set of all permutations of $\{0, \ldots, b-1\}$. The metric is also known as *Earth Mover's Distance* (EMD), because one popular interpretation regards the histograms as piles of dirt, and the Wasserstein metric computes the minimum amount of work to shift one pile into the shape of another. For multi-dimensional histograms, this computation involves the solution of a transportation problem, typically solved with the Hungarian Algorithm. As our histograms are one-dimensional, the formula simplifies to

$$\mathcal{W}(G_b, H_b) = \sum_i \frac{1}{b}\left|\sum_{j \le i} g_b^j - h_b^j\right|, \tag{6}$$

which can be computed in time $\mathrm{O}(b)$ with dynamic programming. The distance metric $\mathcal{W}$ induces a binary classifier L_τ with an arbitrary threshold τ of the form

$$L_\tau(G_b, H_b) = \begin{cases} \text{true} & \text{if } \mathcal{W}(G_b, H_b) \le \tau, \\ \text{false} & \text{otherwise.} \end{cases} \tag{7}$$

This classifier is the motivation and our primary application for the histogram technique. We will show that the classifier – if combined with a suitable point projection function v and threshold τ – serves as a good estimator whether two scans are spatially close.

B. Point Projection Functions

The point projection function not only reduces the computational complexity of the Wasserstein metric, it also has a positive influence on the general robustness of the method. For this, consider a robot revisiting a location. The robot will not retrace its previous path exactly. For instance, an autonomous car cannot travel on the exact same lane in the opposite direction, and the occurring position drift makes it virtually impossible to do so even if traffic safety is not an issue. Thus, we seek the histogram to be resistant against small orientation and position perturbations.

Let p denote a sensor measurement that is projected into three-dimensional space and relative to the point of origin p_0 of the sensor. The range function $v(p) = \|p\|$ assigns to each point it's distance from the sensor origin. This projection function is orientation invariant, but introduces a noticeable distortion in the histogram with position perturbations since the distance is very much dependent on the measuring point of origin p_0. As alternative, we propose the function of height above the ground plane[1] $v(p) = \langle p, u \rangle$. This function is also orientation invariant and much less sensitive to position changes, as a ground vehicle will keep a fairly constant height above ground. The up-vector u can either be fixed as $(0, 0, 1)^{\mathrm{T}}$ or dynamically computed with a principal component analysis of the point cloud, assuming positive z values to point upwards. Unlike the range function, the height function exhibits sensitivity to noise in the roll and pitch orientation. This turns out to be harmless for car-like robots with suspension, but may cause problems with non-suspended vehicles in rough terrain.

C. Thresholding

A good classification performance hinges on the proper distance threshold τ for histograms. The distance metric $\mathcal{W}$ has no immediate physical representation, so it is not obvious what constitutes a good threshold value. However, we can show that the output of the metric is bounded by $[0, 1]$. As can be seen in equation (6), the distance between two histograms is never negative, and it is zero if and only if both histograms are completely identical. Further, we know that $\sum_i h_b^i = 1$ and $h_b^i \geq 0$, which implies that

$$\begin{aligned} 0 \leq \mathcal{W}(G_b, H_b) &\leq \sum_i \frac{1}{b} \left| \max_{G_b} \sum_{j \leq i} g_b^j - \min_{H_b} \sum_{j \leq i} h_b^j \right| \\ &\leq \sum_i \frac{1}{b} |1 - 0| = 1. \end{aligned} \tag{8}$$

A good threshold was derived experimentally ($\approx 10^{-3}$).

IV. Evaluation

A. Singapore Data Sets

Trials for data collection were conducted in Singapore. In these trials, data from a NovAtel SPAN-SE dual-antenna GNSS receiver integrated with an IMU-LCI and from the Velodyne HDL-64E S2 were collected using a modified Toyota SUV driven in dirt-road environments with sometimes limited GNSS coverage. The computers used for data acquisition were time-synchronised using a time server. Camera images were recorded and time-synchronised as well for human consumption. The positioning solution is then post-processed in NovAtel Inertial Explorer to arrive at the ground truth trajectory. Tracks have been recorded from 12 different routes, with one to four tracks per route.

[1]Technically, the plane is anchored in the sensor origin and parallel to the ground. The histogram is thus shifted by the sensor height above ground, which can be compensated at the user's discretion.

Fig. 1. Route A

Fig. 2. Route B

Three main routes were selected with typical navigation strategies: Route A (figure 1) represents a simple U-turn or go-home scenario. Routes B (figure 2) and Route C (figure 3) are more complex urban and rural exploration scenarios. We have a good GPS solution as ground truth for all three routes.

B. Threshold Determination

Our classifier has a single threshold parameter τ which needs to be learned. As ground truth, we consider two locations as the same if their Euclidean distance according to the GPS localization falls below $d = 10\mathrm{m}$. This distance selection has a big impact on the classification results. Decreasing this distance generally improves the classifier

Fig. 3. Route C

performance. If we were to set $d = 0\mathrm{m}$, our classificator would achieve almost perfect precision and recall because each scan – discounting measurement noise – would need only to match itself. We selected the distance threshold based on the the fact that it is approximately the width of two road lanes in Singapore. Given that the effective measuring range for the scan registration in our SLAM framework is determined to be about $50\mathrm{m}$, we feel that the value of d is chosen adequately.

For each data set, we computed the $\mathcal{W}$ metric for each possible pair of scans. Using the ground truth position data, we determined if the classifier would yield a True Positive (TP), False Positive (FP), True Negative (TN), or False Negative (FN) for different thresholds τ. Then, we evaluated the classification performance with the F_1 measure

$$\mathrm{F}_1 = \frac{2 \cdot \mathrm{TP}}{2 \cdot \mathrm{TP} + \mathrm{FN} + \mathrm{FP}} \tag{9}$$

and the Matthews Correlation Coefficient

$$\mathrm{MCC} = \frac{\mathrm{TP} \cdot \mathrm{TN} - \mathrm{FP} \cdot \mathrm{FN}}{\sqrt{(\mathrm{TP} + \mathrm{FP})\,(\mathrm{TP} + \mathrm{FN})\,(\mathrm{TN} + \mathrm{FP})\,(\mathrm{TN} + \mathrm{FN})}}. \tag{10}$$

We selected the F_1 measure because it is a widely used performance metric for classification. However, we feel that the MCC measure is more relevant for our data sets, because our test sets contain many more negative examples than positive ones. The MCC measure is designed to counteract this imbalance, which is why the MCC values are generally slightly worse than the F_1 values.

C. Singapore Classification Results

As detailed in table I, we optimized the threshold τ for the best possible classification performance by separating the data into a training set and a test set and then evaluating the performance. The τ values are of similar orders of magnitude and exhibit a good performance in our chosen measures. The range projection function generally performs worse than the height function in our data sets, with the notable exception of Route A. This is most likely because that particular track is surrounded by obstacles of very similar height, but with different distances to the road. Further, we traveled the exact same trajectory twice, so there is very little position drift between subsequent visits of the same location. In a second experiment, we showed that the classifier performs well even if the threshold τ is not learned from the same data set. For this experiment, we chose different thresholds throughout the full range of learned values and re-evaluated our data sets as detailed in table II. All values are evaluations with the height function. The entry labeled "Worst Case" refers to the worst classification results we encountered in any of our data sets, including those that had minor issues with the GPS ground truth data and were excluded from the presentation in this paper. The results are consistently good for all thresholds and data sets, indicating a fairly robust classifier. This is also reflected in the Receiver Operating Characteristic (ROC) curve (figure 4), which plots the False Positive Rate against the True Positive Rate. The former is roughly proportional to the magnitude of the threshold τ. The curve is averaged over all data sets.

Data Set	Projection	Optimal τ	F_1	MCC
Route A	Height	0.00487	0.929	0.922
Route A	Range	0.00610	0.936	0.927
Route B	Height	0.00512	0.914	0.913
Route B	Range	0.00380	0.890	0.891

TABLE I

THRESHOLD DETERMINATION FOR DIFFERENT DATA SETS AND PROJECTION FUNCTIONS

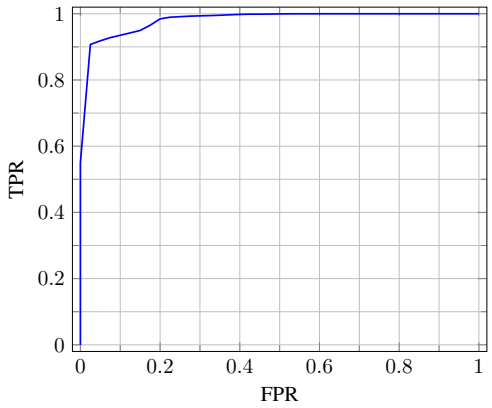

Fig. 4. Receiver Operating Statistic for the classifier

Data Set	$L_{0.003}$	$L_{0.004}$	$L_{0.005}$	$L_{0.006}$	$L_{0.007}$
Route A	0.899	0.910	0.921	0.908	0.886
Route B	0.897	0.905	0.913	0.907	0.887
Route C	0.950	0.960	0.951	0.957	0.936
Worst Case	0.668	0.893	0.910	0.898	0.862

TABLE II

MCC FOR CLASSIFICATION WITH DIFFERENT THRESHOLDS

D. Magnusson Data Sets

Magnusson et al. evaluate their algorithm on three data sets which are available at the Osnabrück Robotic 3D Scan Repository [16]. An in-depth description of the data sets can be found there. The *Hannover2* data set consists of 924 omnidirectional laser scans recorded at the Campus of the Leibniz University Hannover. It contains several loop closures in an outdoor environment. The *AASS* data set was recorded inside the AASS building at the Örebrö University in Sweden. It includes 60 omnidirectional laser scans forming a loop topologically similar to Route A of the Singpapore Data Set. The *Kvarntorp* data was recorded inside the Kvarntorp mine near Örebrö in Sweden. Out of four independent robot missions we use the fourth followed by the first. Those missions overlap each other, leading to several loop closures. The resulting data set consists of 131 scans, each covering a 180° horizontal field of view. The environment inside the mine is highly self-similar, posing an additional challenge.

We use the ground truth as proposed by Magnusson et al [15], a ground truth similarity matrix computed

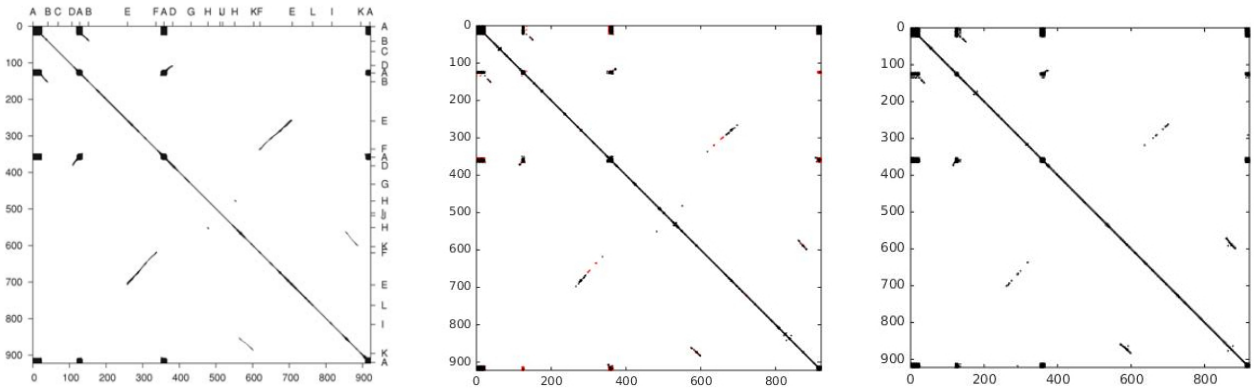

(a) Ground Truth (b) Our histograms (c) NDT histograms

Fig. 5. Hannover2 data set: (a) shows the ground truth similarity matrix, overlapping scans are marked black. (b) presents our LIDAR histograms, black the height function and red the range function (red labels are partly overwritten by black labels) with thresholds $\tau = 0.0033,\ 0.004$, respectively. (c) shows the result of Magnusson et al [15], overlapping scans are marked black.

from the matrix of distances between all scan pairs. For the *Hannover2* and *Kvarntorp* data sets, all scans which are at most $3\mathrm{m}$ apart are marked as overlapping. The *AASS* data set uses a smaller distance threshold of $1\mathrm{m}$, as it is an indoor scenario with significant occlusion by doors and hallways. In the *Kvarntorp* data set, scan direction has to be taken into account as the scans are not omnidirectional. The threshold is chosen at $20°$ orientation difference.

E. Comparison

We ran the data sets with both the NDT-based algorithm and our own. We manually fine-tuned the threshold τ for both algorithms to achieve optimal results. We were able to reproduce the results from [15], albeit with slightly different threshold values. Similar to the Singapore data sets, the height histogram performed slightly better in general than the range histogram. However, there are a few notable exceptions where the range histograms detected loop closures which the height histograms missed. We highlighted those instances in red.

On the *Hannover2* data set (figure 5) we achieve a similarity matrix that, based on visual inspection, comes very close to the ground truth. Compared to the NDT algorithm, our results are of the same if not slightly better quality. The same holds for the *AASS* loop (figure 6). Our results are of at least the same quality, showing a higher robustness around scan 45 where the NDT algorithm detects false positives.

As expected the Kvarntorp data set proves to be challenging (figure 7), resulting in one false positive detection of a loop closure for scans 15 (location C) and 64 (location B). The environments at the respective locations are indeed highly similar, explaining this false detection. The loop closure between location A and B around scans 5 and 60 on the other hand is not detected at all. In this case, the NDT algorithm proves to be more reliable, producing no false positive and detecting all loop closures.

We compared the algorithm performances on an Intel Core i7 3.2 GHz with 12 GB RAM. Table III shows the average run times on a single scan of each data set. The increased complexity of NDT translates to a noticeable performance penalty. Once the histograms have been created though, the comparison of two histograms takes roughly the same time for NDT ($15\,\mu\mathrm{s}$) and our method ($13\,\mu\mathrm{s}$).

	Hannover2	AASS	Kvarntorp
Magnusson	0.36	1.059	0.795
Height	$9.994 \cdot 10^{-3}$	0.069	0.063
Range	$1.209 \cdot 10^{-3}$	$7.917 \cdot 10^{-3}$	$6.936 \cdot 10^{-3}$

TABLE III
AVERAGE HISTOGRAM CREATION TIME PER SCAN IN SECONDS

V. CONCLUSION

The loop closure detection algorithm has been shown to exhibit high precision and recall and is considerably fast for real-time UGV applications. We have shown that relatively simple descriptor primitives such as range and height measurements constitute a powerful classificator which competes with computationally more expensive methods such as NDT-based histograms. However, unlike NDT, our approach is not applicable to scan registration itself; other algorithms are required to re-localize the robot and achieve global convergence. Given that loop closures are relatively rare events, we consider this a desirable trade-off.

LIDAR histograms are expressive descriptors for scene characteristics, and we believe that they can be applied successfully to scene recognition problems in general. Each histogram can be interpreted as a sample from a Dirichlet distribution. Preliminary tests suggest that it is possible to learn Dirichlet models or Dirichlet mixture models of scanned areas, yielding a compact representation of different environments. Apart from the potential improvement to our loop closure detector, the ability to distinguish different environment types may help to select appropriate navigation strategies and behaviors for autonomous systems.

ACKNOWLEDGEMENT

We wish to thank Martin Magnusson (AASS) who generously provided us with his NDT histogram source code, and Stephen Chai Kian Ping (DSO National Labs) for his

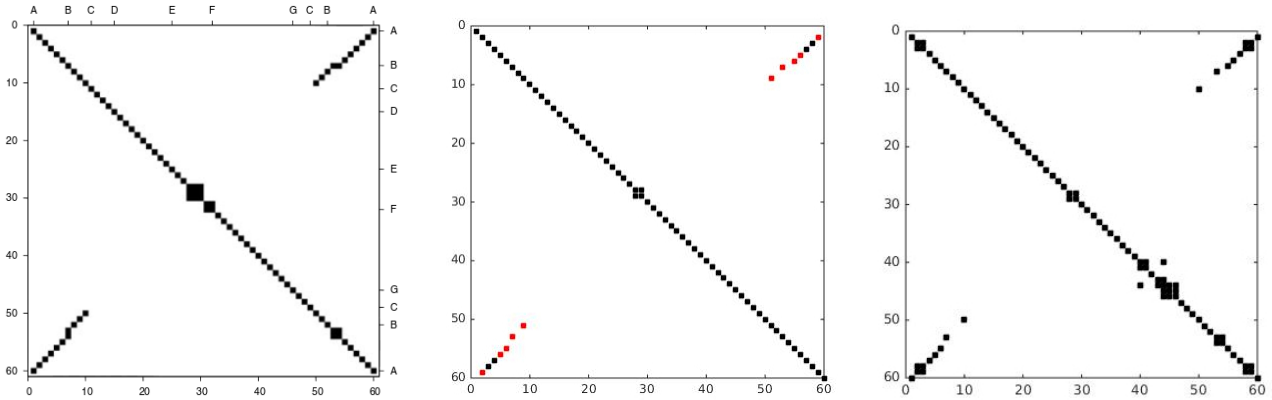

(a) Ground Truth (b) Our histograms (c) NDT histograms

Fig. 6. AASS data set: (a) shows the ground truth similarity matrix, overlapping scans are marked black. (b) presents our LIDAR histograms, black the height function and red the range function (red labels are partly overwritten by black labels) with thresholds $\tau = 0.0027,\ 0.0045$, respectively. (c) shows the result of Magnusson et al [15], overlapping scans are marked black.

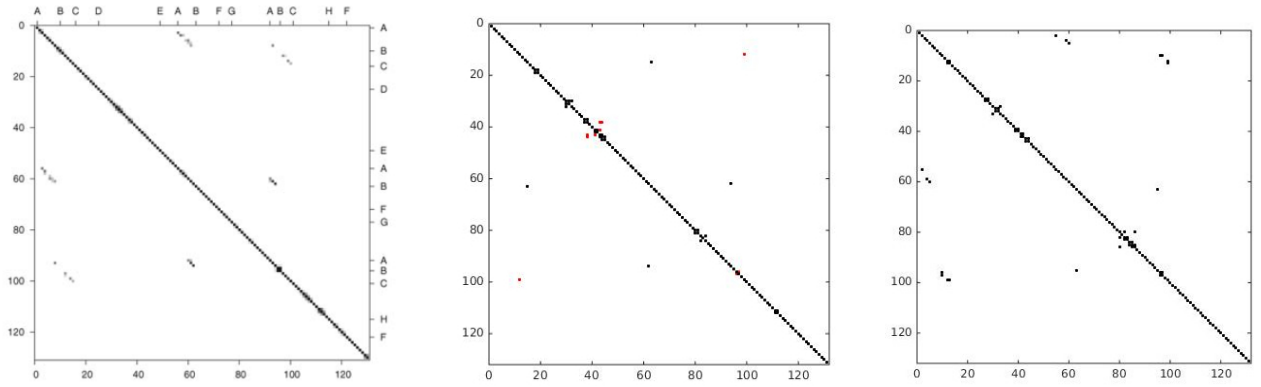

(a) Ground Truth (b) Our histograms (c) NDT histograms

Fig. 7. Kvarntorp data set: (a) shows the ground truth similarity matrix, overlapping scans are marked black. (b) presents our LIDAR histograms, black the height function and red the range function (red labels are partly overwritten by black labels) with thresholds $\tau = 0.0018,\ 0.0042$, respectively. (c) shows the result of Magnusson et al [15], overlapping scans are marked black.

outstanding work in compiling the Singapore Data Sets and numerous insightful discussions.

REFERENCES

[1] Y. Bar-Shalom and T. Fortmann, *Tracking and Data Association*. Academic Press (Boston), 1988, iSBN-13: 978-0-120-79760-8.

[2] D. Lowe, "Distinctive image features from scale-invariant keypoints," *International Journal of Computer Vision*, vol. 60, no. 2, pp. 91–110, November 2004.

[3] H. Bay, A. Ess, T. Tuytelaars, and L. Van Gool, "SURF: Speeded up robust features," *Journal of Computer Vision and Image Understanding (CVIU)*, vol. 110, no. 3, pp. 346–359, June 2008.

[4] K. Konolige and M. Agrawal, "FrameSLAM: From bundle adjustment to real-time visual mapping," *IEEE Transactions on Robotics*, vol. 24, no. 5, pp. 1066–1077, October 2008.

[5] M. Agrawal and K. Konolige, "CenSurE: Center surround extremas for realtime feature detection and matching," in *Proceedings of the 10th European Conference on Computer Vision*, 2008, pp. 102–105.

[6] J.-S. Gutmann and K. Konolige, "Incremental mapping of large cyclic environments," in *Proceedings of IEEE International Symposium on Computational Intelligence in Robotics and Automation (CIRA)*, 1999.

[7] J. Sprickerhof, A. Nüchter, K. Lingemann, and J. Hertzberg, "An explicit loop closing technique for 6D SLAM," in *Proceedings of 4th European Conference on Mobile Robots*, 2009.

[8] J. Neira and J. Tardos, "Data association in stochastic mapping using the joint compatibility test," *IEEE Trans. Robot. Autom.*, vol. 17, no. 6, pp. 890–897, December 2001.

[9] J. Nieto, J. Guivant, and E. Nebot, "Real time data association for FastSLAM," in *Proceedings of IEEE International Conference on Robotics and Automation (ICRA)*, 2003.

[10] S. Wijesoma, L. Perera, and M. Adams, "Toward multidimensional assignment data association in robot localization and mapping," *IEEE Transactions on Robotics*, vol. 2, no. 2, pp. 350–365, 2006.

[11] T. Bailey, E. Nebot, J. Rosenblatt, and H. Durrant-Whyte, "Data association for mobile robot navigation — a graph theoretic approach," in *Proceedings of IEEE International Conference on Robotics and Automation (ICRA)*, 2000.

[12] B. Stewart, J. Ko, D. Fox, and K. Konolige, "The revisiting problem in mobile robot map building: A hierarchical bayesian approach," in *Proc. of 19th Conf. on Uncertainty in Artificial Intelligence*, 2003.

[13] P. Pfaff, R. Triebel, and W. Burgard, "An efficient extension to elevation maps for outdoor terrain mapping and loop closing," *International Journal of Robotics Research*, vol. 26, no. 2, February 2007.

[14] J. Folkesson and H. Christensen, "Closing the loop with graphical slam," *IEEE Transactions on Robotics*, vol. 23, no. 4, pp. 731–741, August 2007.

[15] M. Magnusson, H. Andreasson, A. Nüchter, and A. J. Lilienthal, "Automatic appearance-based loop detection from three-dimensional laser data using the normal distributions transform," *Journal of Field Robotics*, vol. 26, no. 11–12, pp. 892–914, December 2009.

[16] A. Nüchter and K. Lingemann, "Osnabrück robotic 3d scan repository," http://kos.informatik.uni-osnabrueck.de/3Dscans/, 2011, [Online; accessed July 13, 2015].